CFD Study of Three-Dimensional Dynamic Stall of Various Planform Shapes

A. Spentzos, G.N. Barakos, K.J. Badcock and B.E. Richards

CFD Laboratory
Department of Aerospace Engineering
University of Glasgow
Glasgow G12 8QQ, United Kingdom
www.aero.gla.ac.uk/Research/CFD/projects/DS

Keywords: Unsteady Aerodynamics, Omega Vortex, Rotorcraft CFD, Dynamic Stall

Abstract

Numerical simulations of the three-dimensional dynamic stall phenomenon have been undertaken using Computational Fluid Dynamics. As a first step, validation calculations have been performed for cases where experimental data were available. Although, the amount and quality of the experimental data available for three-dimensional dynamic stall is much less than what is available for two-dimensional cases, the CFD was found capable of predicting this complex three-dimensional flow with good accuracy. Once confidence on the CFD method was established, further calculations were conducted for a wing planform closer to a helicopter blade. The calculations revealed the detailed structure of the three-dimensional dynamic stall vortex and its interaction with the tip vortex. Remarkably, strong similarities in the flow topology were identified for wings of very different planforms. It also appears, that the geometry of the tip has a significant influence on the formation and evolution of the three-dimensional dynamic stall flow.

Nomenclature

c	Chord length of the aerofoil
C_p	Pressure coefficient, $C_p = \frac{1}{2\rho U_\infty^2 S}(p - p_\infty)$
C_L	Lift coefficient, $C_L = \frac{L}{2S\rho U_\infty^2}$
d	Distance along the normal to chord direction
x	Chord-wise coordinate axis (CFD)
y	Normal coordinate axis (CFD)
z	Span-wise coordinate axis (CFD)
k	Reduced frequency of oscillation, $k = \frac{\omega c}{2U_\infty}$
L	Lift force
M	Mach number
p	Pressure
Re	Reynolds number, $Re = \rho U_\infty c/\mu$
t	Non-dimensional time
u	Local streamwise velocity
U_∞	Free-stream velocity

Greek

α^+	Nondimensional pitch rate, $\alpha^+ = \frac{d\alpha}{dt}\frac{c}{U_\infty}$
α	Instantaneous incidence angle
α_0	Mean incidence angle for oscillatory cases
α_1	Amplitude of oscillation
ρ	Density
ρ_∞	Density at free-stream
ω	Angular frequency
ϕ	Phase angle

Acronyms

AR	Apect Ratio
CFD	Computational Fluid Dynamics
ELDV	Embedded Laser Doppler Velocimetry
DS	Dynamic Stall

1 Introduction

The phenomenon of dynamic stall is cental in rotorcraft aerodynamics and has so far be investigated by various authors. A review up to 1996 of all CFD efforts related to DS has been provided by Ekaterinaris and Platzer [1, 2]. Several other papers have appeared in the literature [3] and the reader could consult the recent paper by Barakos and Drikakis [4] for an update. A literature survey indicated that since 1950 only three CFD investigations attempted to make the step from 2-D to 3-D simulation of DS with little evidence of success. Newsome [5] focused on the laminar flow regime and attemted to simulate the experiments of Schreck and Helin [6]. Newsome's work predicted the 3D dynamic stall vortex but provided very little information regarding the interaction of this vortex with the tip vortex of the wing. This interaction, as we will show in this work, is important. The work by Morgan and Visbal [7] considered the oscillatory motion of a square wing at laminar flow conditions with end plates at both tips. The objective was to approximate the conditions inside a wind tunnel with the model spaning the test section. This work was focused on the development of vorticity near the wing surface. The work of Ekaterinaris [8] is the most recent in 3-D DS but to a great extend deals with 2-D configurations and the 3-D problem is provided as a demonstration of the capabilities of CFD. Regardless of the lack of CFD investigations, experimental works on 3-D dynamic stall were more successful. Table 1, provides a summary of all works the authors have identified in the literature, along with the flow conditions, measured quantities and experimental techniques. One cannot fail to notice that pressure measurements dominate while flow visualisation and velocity profile measurements are rare. In addition, no data or no measurements have been conducted for wings of high aspect ratio. It is evident from Table 1 that all experimental effort was devoted to the study of the fundamental unsteady aerodynamics problem of DS. The literature survey revealed no experimental works on high aspect ratio twisted wings which are obviously closer to helicopter blades. In the present work two objectives have been set: i) to validate a CFD method for 3-D DS and ii) to investigate the flow topology during the evolution of 3-D dynamic stall over various wing planforms. The paper is organised as follows. A brief description of the method is first presented which is followed by a description of three selected validation cases. For each case, the original experimental data have been obtained and effort has been made to simulate the experiment as accurately as possible. The experiments and the CFD results are post-processed and presented in exactly the same way in order to facilitate comparisons. The validation cases are complimented with an additional case of a high aspect ratio twisted wing, which better approximates a real helicopter blade. After this analysis, conclusions are drawn and suggestions are put forward for future investigations.

2 Numerical Method

The details of the employed CFD solver can be found in [9], only a summary is given in this paper. The code is capable of solving flow conditions from inviscid to fully turbulent using the Reynolds Averaged Navier-Stokes (RANS) equations in three dimensions. Dettached eddy simulation and large eddy simulation options are available though these were not used in this work. Due to the flow conditions considered here, simple two-equation turbulence models have been employed. Most of the results presented in this paper have been obtained using the baseline $k - \omega$ model [10]. To solve the RANS equations, multi-block grids were generated around the required geometries, and the equations were discretised using the cell-centered finite volume approach. For the discretisation of the convective fluxes Osher's scheme has been used. A formaly third order accurate scheme is achieved using a MUSCL interpolation technique. Viscous fluxes were discretised using central differences. Boundary conditions were set using two layers of halo cells. The solution was marched in time using an implicit second-order scheme and the final system of algebraic equations was solved using a preconditioned Krylov subspace method.

3 Validation Cases

At present, three validation cases have been selected for computations out of the experimental investigations presented in Table 1. The first case concerns the flow visualisation experiments conducted by Moir and Coton [11] at the smoke tunnel of the University of Glasgow. The second validation case was based on the experiments conducted at the S1L wind tunnel of the University of Marseilles' and are detailed in [12, 13]. A third valiation case was based on the experiments by Coton and Galbraith [14] conducted at the Handley-Page wind tunnel of the University of Glasgow. A summary of the flow conditions of all validation cases along with the quantities measured in the experiments is presented in Table 1. The cases were selected so that a wide range of conditions is covered including laminar and turbulent flow, oscillating and ramping wing motions and several planforms. In addition to the above cases CFD calculations have also been undertaken for a fourth planform, although for this last case no experimental data are available. In contrast to the previous cases were untwisted short aspect ratio wings have been employed, the fourth case deals with a high aspect ratio twisted wing which is a better approximation to a helicopter rotor blade. For all selected cases the details of the employed CFD grids along with the CPU time required for computation are presented in Tables 2 and 3, respectively.

3.1 The flow visualisation experiments by Moir and Coton

The flow visualisation experiments by Moir and Coton [11], provided detailed account of the initiation and evolution of the DS vortex at laminar flow conditions ($Re = 13,000$). The employed wing was of rectangular planform with rounded tips and of an aspect ratio of 3. A schematic of this planform is shown in Figure 1(a). The wing had a NACA 0015 section along the span. Although both oscillatory and ramping wing motions were considered during experiments [11], CFD calculations have been performed for a ramping case only with a reduced ramping rate of $\alpha^+ = 0.16$. The low Reynolds number of this experiment was beneficial since smoke visualisation can be made clearer at lower wing speeds and from the point of view of CFD no turbulence modelling is necessary. A set of still images has been extracted from the tapes recorded during the experiments and were consequently used for comparisons with the CFD simulation. Figures 2 and 3 present the comparison between experiments and simulation at incidence angles where, as perceived by the authors, the most important features of the 3-D DS are shown. Figure 2(a), shows the plan view of the wing at an incidence angle of 30^o. At this stage, the DSV is well formed and its inboard portion is located at approximately 1/3 of chord from the leading edge, running parallel to the pitch axis of the wing. The portion however, of the DSV close to the tips, is deflected towards the leading edge, and appears to interact with the tip vortices. Further aft, one can also see the trailing edge vortex, whose ends tend to merge with the DSV and the tip vortices. At this stage the trailing edge vortex is of comparable size with the DSV. Figure 2(b), shows the same time instance from a different viewing angle, but where streamlines have been seeded at different locations in order to elucidate the merging of the DSV with the tip vortices, as well as the backwards tilted arch-like shape of the DSV resembling that of an inclined Ω. Figure 3(a) is a plan view of the Ω-shaped vortex an an incidence of 40^o. One can see that the streamlines closer to the surface of the wing have the same circular pattern as the smoke streaks of the visualisation. This points out to the fact that that the DSV impinges on the surface of the wing at a distance of a chord length inboards from the tips at the spanwise direction, and at half a chord's length in the chordwise direction. The trailing edge vortex can no longer be seen, as by that stage it has been shed in the wake pushed by a continuously growing in size DSV, which is constantly fed with momentum by the free stream and the wing motion. A front view of the same vortical structure can be seen in Figure 3(b). This view reveals a remarkable agreement between experiments and computation as far as the extend and shape of the Ω vortex are concerned.

3.2 The ELDV measurements by Berton *et al.*

The DS of an oscillating, tapered, low aspect ratio wing has been studied by Berton *et al.* [12, 13]. This is a very interesting case for two reasons: i) velocity data have been obtained at various phase angles during the oscillation and at several spanwise and chorwise locations and ii) the wing planform resembles an active control surface similar to the ones encountered in modern super-maneuverable aircraft. The experiments [12] were conducted in the S1L high subsonic wind tunnel of the Aerodynamics Laboratory of Marseilles using a novel Embedded Laser Doppler Velocimetry (ELDV) technique. According to this method the laser probe is mounted on the same circular rotating disc which also supports the wing. The shape and dimensions of this planform can be seen in Figure 1(b). The employed wing had a root chord length of 0.24m and was mounted in the axisymmetric wind tunnel octagonal cross section of width equal to 3m. For the cases selected here the freestream velocity was 62.5m/s. Experimental results [13] are available for oscillatory motion of the wing for several mean angles, amplitudes of oscillation between 3^o and 6^o and reduced frequencies in the range of 0.02 to 0.1. Two cases were computed both having a mean angle $\alpha_o = 18^o$ and amplitude $\delta\alpha = 6^o$, while the reduced frequencies considered were k=0.048 and k=0.06. Comparisons of u-velocity profiles at four different phase angles during the oscillation cycle can be seen in Figures 4-6 for k=0.048 and Figures 7-9 for k=0.06. Overall, CFD was found to be in excellent agreement with the experimental measurements. In each of these figures, one can see an embedded plot of the cross spanwise section where the probing station is also shown. The chordwise location of the probe, streamlines, as well as the pressure distributionare presented at the corresponding phase angle. For each of the two reduced frequencies selected for this work, velocity profiles are shown at three stations ($x/c = 0.4$, $z/c = 0.5$), ($x/c = 0.6$, $z/c = 0.5$) and ($x/c = 0.4$, $z/c = 0.7$) for four phase angles (ϕ) of 0, 90, 180 and 270 degrees. The velocity profiles at phase angles of 0 and 270 degrees reveal a fully attached flow at all spanwise and chordwise stations. In contrast, the velocity profiles at 90 and 180 degrees show massive recirculation of the flow. This can also be seen from the embedded plots at Figures 4 to 9. It is remarkable that the CFD solution predicted the onset and the extend of the separation very well. It is only for the inboard station at $x/c = 0.6$ that the CFD slightly under-predicts the reparation at a phase angle of 180 degrees. It is also interesting that the CFD results predict very well the velocity profiles at the outboard station of $z/c = 0.7$ for all phase angles and employed reduced frequencies. As will be discussed in subsequent paragraphs, the flow near the tip is highly 3-D. In this region, the DS vortex appears to interact with the tip vortex resulting in a very complex flow field. For this case the CPU time was found to be higher apparently due to the extra resolution required near solid boundaries and the overhead of the employed turbulence model.

3.3 The pressure measurements of Coton and Galbraith

The tests described here [14], were carried out in the 'Handley Page' wind tunnel of the University of Glasgow which is of low speed closed-return type. The planform of the wing model used for this experiment is shown in Figure 1(a). The mode had a chord length of 0.42m, a span of 1.26m and was mounted horizontaly in the tunnel's octagonal cross section of 2.13m x 1.61m. In contrast to other experimental investigation where half-span models are used, Coton and Galbraith [14] used a full-span model with rounded tips. Their model was instrumented with a series of 180 pressure taps grouped in six spanwise locations. In addition, a set of 12 taps was located closer to the tip region. All signals were fed to a datalogging system, at sampling frequences ranging from 218 Hz to 50,000 Hz, depending on the speed of the wing motion of each case. The experimental data used for this work are averaged from a number of consecutive cycles.

For the CFD investigation both ramping and oscillatory cases have been sellected from the database provided by Coton and Galbraith [14]. Figure 10 presents the time history of the geometric incidence as recorded during the experiment. As can be seen, the idealisation of the ramping profile $\alpha = \alpha_o + \alpha t$ usualy employed in CFD calculations is far from satisfactory. In the present work, the time history of the incidence had to be curve-fitted and then sampled according to the desired timestep for each calculation. Several ramping cases have computed and results are presented here for two cases. Both cases were computed at the same Reynolds and Mach numbers of 1.5×10^6 and 0.16 respectively. The reduced pitch rates, however, were $\alpha^+ = 0.011$ and $\alpha^+ = 0.022$. For both cases the incidence varied between -5 and 39 degrees.

Figure 10(b) suggests that a similar treatment is required for the oscillatory cases. The ideal case $\alpha = \alpha_o + \alpha_1 sin(kt)$ had to be generalised so that the imposed wing actuation corresponds the experimental one. It was found that about ten harmonics were necessary and the resulting actuation was described by:

$$\alpha = \alpha_o + \sum_{i=1}^{i=10} \alpha_i sin(ikt)$$

To allow comparisons with the ramping cases the Reynolds and Mach numbers were kept the same. Again, two reduced frequencies were used as fundamental harmonics of the oscillation, namely, $k = 0.092$ and $k = 0.17$.

Comparisons between experiments and CFD results for the surface pressure coefficient are presented in Figures 11 and 12 for the ramping and Figure 13 for the oscillatory cases.

Figure 11 presents the comparison at two incidence angles. One cannot fail to notice that at low incidence (20^o in Figure 11(a)) the experiments and CFD agree quite well. The shape of the Cp contours corresponds to attached flow and the suction peak near the leading edge as well as the pressure recovery along the chordwise direction are adequately captured. Since the wing is loaded, the Cp contours near the tip are distorted due to the presense of the tip vortex. Unfortunately, the number of pressure tabs used for the experiment does not allow for detailed comparison in the near tip region. A dashed line on the Cp plot of the CFD solution indicates the area covered by the pressure taps. A grid is shown on the experimental plot which indicates the location of the pressure taps on the wind tunnel model. At higher incidence angles, the agreement between experiments and CFD was less favourable. A correction of the incidence angle of about 5^o was necessary in order to have a similar loading of the wing. As can be seen in Figure 11(b) both experiments and CFD indicate the presense of a massive vortical structure over the wing. This can be seen near the centre of the plot at a spanwise location z/c of 0.75 where a local suction peak is present. As will be discussed in subsequent paragraphs this peak is due to the DS vortex impinging on the wing surface. At this high incidence a strong tip vortex dominates the near tip region of the wing. This is now captured by both experiments and CFD and appears as a secondary suction peak at z/c of about 1.4. This secondary peak corresponds to Cp values of about -3, which is match less than the peak due to the DS vortex which reaches Cp values of -1.2. The experimentalists reported a notable upwash in the tunnel's test section, possibly attributed to the supporting struts of the wing as well as the tunnel wall effects. This upwash was of the order of few degrees and of the same order as the incedence correction applied for comparisons. However, it was not possible to devise a constant correction for all computed cases. As can be seen in Figure 12(b), a smaller correction of 4^o was necessary. This also points out defficiencies in the calculation since it known from 2-D cases [4] that slower actuations of the wing are harder to simulate than rapid ones. This is due to the fact that viscous flow effects are more dominant for low ramp rates (especially as static stall conditions are approached).

Similar remarks can be made for the oscillatory cases for which CFD results are presented in Figure 13. Comparisons are shown only for a phase angle of 90^o which corresponds to the highest incidence encountered during the oscillation. Again the suction peaks induced by the DS and the tip vortices are predicted at almost the same magnitude provided a 4^o correction of the incidence was applied.

4 Investigation of Flow Topology

Having obtained a flow-field similar to the one indicated by the flow visualisation of Moir and Coton [11] and having established confidence on the prediction of the velocity [12, 13] and surface pressure fields [14] during 3-D dynamic stall, emphasis is now placed on the analysis of the obtained results and the evolution of the flow-field. To complement the calculations conducted so far, an additional case had been studied. For this case no experimental data were available for comparisons. A wing of aspect ratio ten and a linear twist of -10^o was considered. Since all previous calculations were conducted for low aspect ratio wings, it was expected that the evolution of dynamic stall would be quite different for wings of higher aspect ratio. Surprisingly, this was not the case.

In all cases investigated, it appears that the evolution of the DS phenomenon appears to follow certain rules. Dynamic stall starts with the production of a large vortical structure which is energised by both the free stream and the wing's motion. Figure 14 presents surface Cp contours (left) as well as contours of streamwise velocity component (right) slightly above the wing surface. This is done for all planforms. In this figure, negative u-velocity indicates the presence of the DS vortex, since its direction of rotation is clockwise for a freestream in the positive x-direction. In all cases shown, the inboard portion of the DS vortex appears to be parallel to the trailing edge, while its outboard portion approaches the leading edge part of the tip. However, one distinctive difference has been observed for the low aspect ratio wing with rounded tips. For this case, the DS vortex was terminated inboards of the wing tip in the region where it impinged on the wing surface. This was not the case for the high aspect ratio and the tapered wings where the DS vortex appears to be connected to the tip vortex near the leading edge of the wing. The above remarks are further supported by Figure 15, which shows the streamlines and the vortex cores for the three planforms at the stall angle. Again, in the cases of the tapered and high aspect ratio wings the DS vortex appears to be connected with the tip vortex near the leading edge, this in no longer occuring in the case of the low aspect ratio wing. The same configuration with the DS vortex impinging almost verticaly on the wing applies in the latter case as observed in Figures 2 and Figure 15. For the low Reynolds number case shown in Figure 2 and Figure 3, the DSV and tip vortices also appear to be connected at the leading edge near the tip. That points out that this effect is a combination of two parameters, the Reynolds number and the shape of the wing tip, as both the tapered and long AR wings had flat tips. This was also observed by the authors in a previous investigation [15] were the DS of low aspect ratio wings was studied. Also, thinking along the line of the vortex theorems of Helmholtz, both configurations seem valid, as vortices either extend to infinity, merge with other vortices or end on solid surfaces. Whatever the shape of the tip was, the DSV was found to approach the leading edge of the tip forming a sharp bend. The exception was found to be the case of the long aspect ratio wing which, however, had a linear negative twist. In this case (see Figure 15(c)), the tip vortex is relatively weaker than in the other two cases, since the tip was exposed to a flow at a lower incidence.

The DSV and the tip vortices have the same direction of rotation, with the right hand side tip vortex inducing a counter clockwise flow as seen in Figure 15. Thus, it is expected that the tip vortex in the area above the leading edge of the tip will induce a crossflow directed inboards. The intencity of this crossflow forces the DSV to bend towards the wing surface, and since the tip vortex on the long aspect ratio wing was relatively weaker due to the negative twist, the DSV bends towards the leading edge of the tip in a smoother fashion as shown in Figure 15(c). Another observation involves the topology of the Cp contours in the near the tip region which appears to follow very similar configurations in all cases, as shown in Figure 14. This points out to the fact that the flow close to the tip is primarily dictated by the presense of the tip vortex.

5 Conclusions and Future Work

Detailed validation of a CFD method has been undertaken for 3D dynamic stall cases. This is the first time in the literature that extensive computations have been undertaken for this very complex unsteady flow phenomenon. The first encouraging result is that CFD was able to match the available experimental data with good accuracy, and moderate computational cost. For the laminar test cases, all flow structures identified with the smoke visualisation were present in the CFD solutions and the flow topology was found to be predicted with remarkable precision. The tapered wing case of the Laboratory of Marseilles [12] was predicted extremely well given the fact that velocity profiles were compared at various ϕ angles during the oscillation of the wing and at various spanwise locations. The ramping cases by Coton and Galbraith [14] were predicted reasonably well with some discrepencies in the stall angle attributed to experimental errors and the presence of the wind tunnel walls which were not taken into account for this simulation. The most remarkable conclusion of this work is the almost universal configuration obtained for the 3D dynamic stall vortex and the tip-vortex for all planforms investigated. It appears that the tip and the Ω-shape vortex form a Π-Ω configuration regardless of the planform shape, provided of course that conditions for dynamic stall are achieved. Several issues remain to be investigated and consequently some future steps are to be undertaken. These include the investigation of the turbulence modelling and simulation aspects of the current CFD solver and the identification of the most promising technique for turbulent flow simulations. Calculations are currently underway with Dettached Eddy Simulation as well as Large Eddy Simulation in order to reveal limitations, if any, in the RANS approach employed in this work. The issues of transition also need a separate investigation.

In addition to the above, a full parametric study of the 3D dynamic stall phenomenon is underway. This is targetting the effects of sideslip, rotation, Mach and Reynolds numbers, geometric twist, aspect ratio and wing-tip shape. Out of this data an indicial model is to be constructed which will serve as an efficient tool for industrial application in aeromechanics simulation codes and possibly real-time simulators. In parallel, the investigation of the flow topology and the vortical interaction encountered during this phenomenon is an ongoing process.

Acknowledgements
Financial support from EPSRC (Grant GR/R79654/01) is gratefully acknowledged. The authors are grateful to prof. Frank Coton of the Department of Aerospace Engineering of the University of Glasgow for providing the experimental data used in paragraphs 3.1 and 3.3.

6 Bibliography

1. EKATERINARIS, J. A., *et al.*, Present Capabilities of Predicting Two-Dimensional Dynamic Stall, AGARD Conference Papers CP-552, Aerodynamics and Aeroacoustics of Rotorcraft, August 1995.

2. EKATERINARIS J.A. and PLATZER M.F., Computational Prediction of Airfoil Dynamic Stall, *Progress in Aerospace Sciences*, **33**(11-12), pp. 759-846 Nov-Dec 1997.

3. VISBAL M.R., Effect of Compressibility on Dynamic Stall, *AIAA Paper 88-0132*, 1988.

4. BARAKOS G.N., and DRIKAKIS D., Computational Study of Unsteady Turbulent Flows Around Oscillating and Ramping Aerofoils, *Int. J. Numer. Meth. Fluids*, **42**(2), pp. 163-186, May 2003.

5. NEWSOME R. W., Navier-Stokes Simulation of Wing-Tip and Wing-Juncture Interactions for a Pitching Wing, *AIAA Paper 94-2259*, 24th AIAA Fluid Dynamics Conference, Colorado Springs, Colorado, USA, June 20-23 1994.

6. SCHRECK S.J. and HELIN H.F., Unsteady Vortex Dynamics and Surface Pressure Topologies on a Finite Wing, *Journal of Aircraft*, **31**(4), pp. 899-907, Jul-Aug 1994.

7. MORGAN, P.E. and VISBAL M.R., Simulation of Unsteady Three-Dimensional Separation on a Pitching Wing, *AIAA paper 2001-2709*, 31st AIAA Fluid Dynamics Conference and Exhibit, Anaheim, CA, 11-14 June 2001

8. EKATERINARIS, J. A., Numerical Investigation of Dynamic Stall of an Oscillating Wing, *AIAA Journal*, **33**(10), pp. 1803-1808, Oct 1995.

9. BADCOCK, K.J., RICHARDS, B.E. and WOODGATE, M.A. Elements of Computational Fluid Dynamics on Block Structured Grids Using Implicit Solvers, *Progress in*

Aerospace Sciences, **36**(5-6), pp. 351-392, Jul-Aug 2000.

10. WILCOX D.C., Reassessment of the Scale-Determining Equation for Advanced Turbulence Models, *AIAA Journal*, **26**(11), pp. 1299-1310, Nov 1988.

11. MOIR, S., COTON, F.N., 'An examination of the dynamic stalling of two wing planforms', Glasgow University Aero. Rept. 9526, 1995

12. BERTON E., ALLAIN C., FAVIER D. and MARESCA C., Experimental Methods for Subsonic Flow Measurements, in Progress in Computational Flow-Structure Interaction, Haase W., Selmin V. and Winzell B., Eds., Notes on Numerical Fluid Mechanics and Multidisciplinary Design, Vol 81, Springer, pp. 97-104, 2003.

13. BERTON E., ALLAIN C., FAVIER D. and MARESCA C., Database for Steady and Unsteady 2-D and 3-D Flow, in Progress in Computational Flow-Structure Interaction, Haase W., Selmin V. and Winzell B., Eds., Notes on Numerical Fluid Mechanics and Multidisciplinary Design, Vol 81, Springer, pp. 155-164,2003.

14. COTON F.N. and GALBRAITH RAM, An Experimental Study of Dynamic Stall on a Finite Wing, *Aeronautical Journal*, **103**(1023), pp. 229-236, May 1999.

15. SPENTZOS A., BARAKOS G., BADCOCK K., RICHARDS B., WERNERT P., SCHRECK S. and RAFFEL M., CFD Investigation of 2D and 3D Dynamic Stall, presented at the AHS 4th Decennial Specialist's Conference on Aeromechanics, San Francisco, California, Jan. 21-23, 2004.

16. FREYMUTH P., 3-Dimensional Vortex Systems of Finite Wings, *Journal of Aircraft*, **25**(10), pp. 971-972, Oct 1988.

17. HORNER M. B., Controlled Three-Dimensionality in Unsteady Separated Flows about a Sinusoidally Oscillating Flat Plate, *AIAA Paper 90-0689*, 28th Aerospace Sciences Meeting, Reno, Nevada, USA, January 8-11 1990.

18. MCCROSKEY W.J., CARR L.W. and MCALISTER K.W., Dynamic Stall Experiments on Oscillating Airfoils, *AIAA Journal*, **14**(1), pp. 57-63, 1976.

19. BARAKOS G.N. and DRIKAKIS D., Unsteady Separated Flows over Manoeuvring Lifting Surfaces, *Phil. Trans. R. Soc. Lond. A*, **358**, pp. 3279-3291, 2000.

20. BARAKOS G.N. and DRIKAKIS D., An Implicit Unfactored Method for Unsteady Turbulent Compressible Flows with Moving Boundaries, Computers & Fluids, **28**(8), pp. 899-922, 1999.

21. PIZIALI R.A., 2-D and 3-D Oscillating Wing Aerodynamics for a Range of Angles of Attack Including Stall, *NASA Technical Memorandum*, TM-4632, September 1994.

22. TANG D.M. and DOWELL E.H., Experimental Investigation of Three-Dimensional Dynamic Stall Model Oscillating in Pitch, *Journal of Aircraft*, **32**(5), pp.163-186, Sep-Oct 1995.

23. LORBER P. F., and CARTA F. O., Unsteady Stall Penetration Experiments at High Reynolds Number, *AFSOR Technical Report*, TR-87-12002, 1987.

Case	Reference	Conditions	Measurements
1	Schreck & Helin [6]	Ramping motion	Surface pressure
		$Re = 6.9 \times 10^4$, $M = 0.03$	Flow visualisation (dye injection)
		NACA0015, AR=2	
2	Piziali [21]	Ramping and oscillatory motion	Surface pressure
		$Re = 2.0 \times 10^6$, $M = 0.278$	Flow visualisation (micro-tufts)
		NACA0015, AR=10	
3	Moir & Coton [11]	Ramping and oscillatory motions	Smoke visualisation
		Re=13,000, $M = 0.1$	
		NACA0015, AR=3	
4	Coton & Galbraith [14]	Ramping and oscillatory motions	Surface pressure
		$Re = 1.5 \times 10^6$, $M = 0.1$	
		NACA0015, AR=3	
5	Tang & Dowell [22]	Oscillatory motion	Surface pressure
		$Re = 0.52 \times 10^6$, M 0.1	
6	LABM [12]	Oscillatory motion	Boundary layers
		$Re = 3 - 6 \times 10^6$, $M = 0.01 - 0.3$	Velocity profiles
		NACA0012	Turbulence quantities

Table 1: Summary of experimental investigations for 3-D DS.

Case	Blocks	Points on wing	Points on tip	Farfield	Wall distance	Topology
3	40	6750	1800	8 chords	10^{-5} chords	3-D C-extruded
4	20	3375	1800	8 chords	10^{-5} chords	3-D C-extruded
6	36	7800	7200	8 chords	10^{-5} chords	3-D C-extruded
High AR twisted wing	36	10800	2800	8 chords	10^{-4} chords	3-D C-extruded

Table 2: Details of the employed CFD grids.

Case	Size (nodes)	No of processors	CPU time (s)
3	2,268,000	12	1.06×10^5
4 ramping	1,134,000	9	2.3×10^5
4 oscillatory	1,134,000	9	7.9×10^5
6	1,828,000	8	1.15×10^6
High AR twisted wing	2,745,432	16	7.35×10^4

Table 3: Details of the CPU time required for calculations. All calculations were performed on a Linux Beowulf cluster with 2.5GHz Pentium-4 nodes.

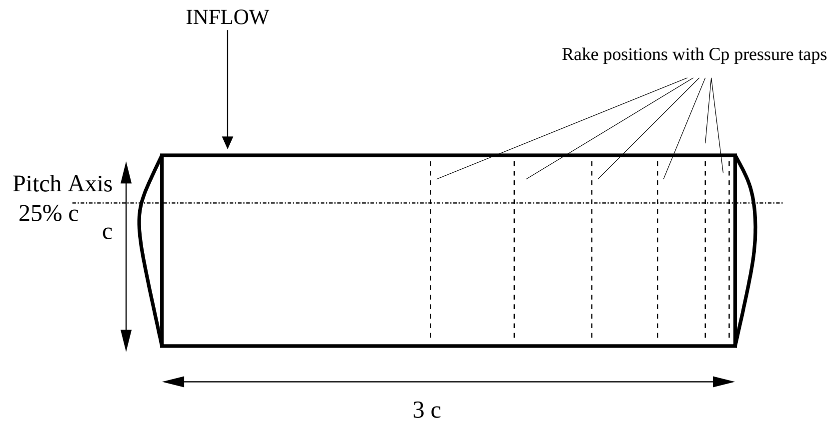

(a) Moir and Coton [11] and Coton and Galbraith [14] (NACA 0012 wing section)

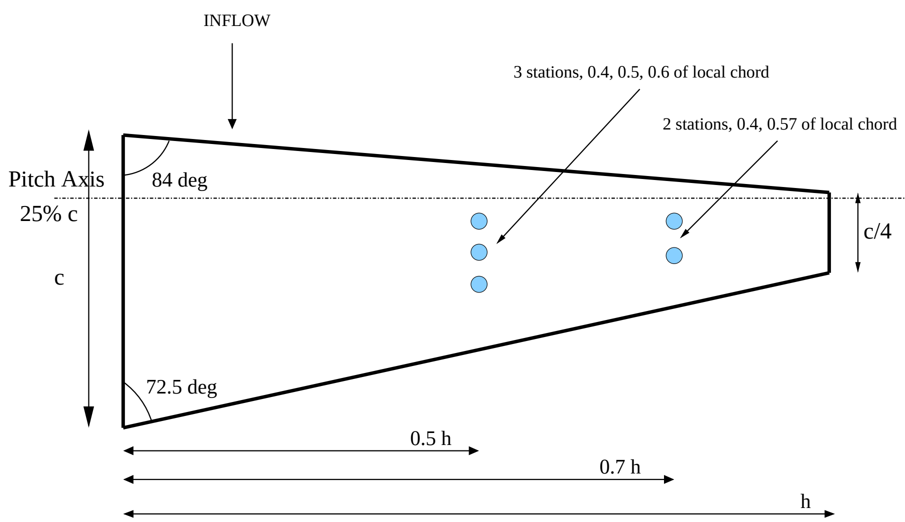

(b) Berton *et al.* [12] (NACA 0012 wing section)

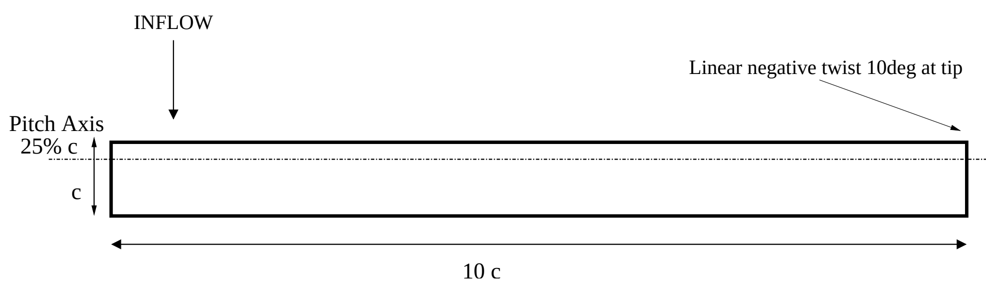

(c) High aspect ratio wing (NACA 0015 wing section)

Figure 1: Wing planforms employed for calculations. (a) Cases 3 and 4 of Table 1 by Moir and Coton [11] and Coton and Galbraith [14]. (b) Case 5 of Table 1 by Berton *et al.* [12]. (c) High aspect ratio wing with linear twist of -10^o.

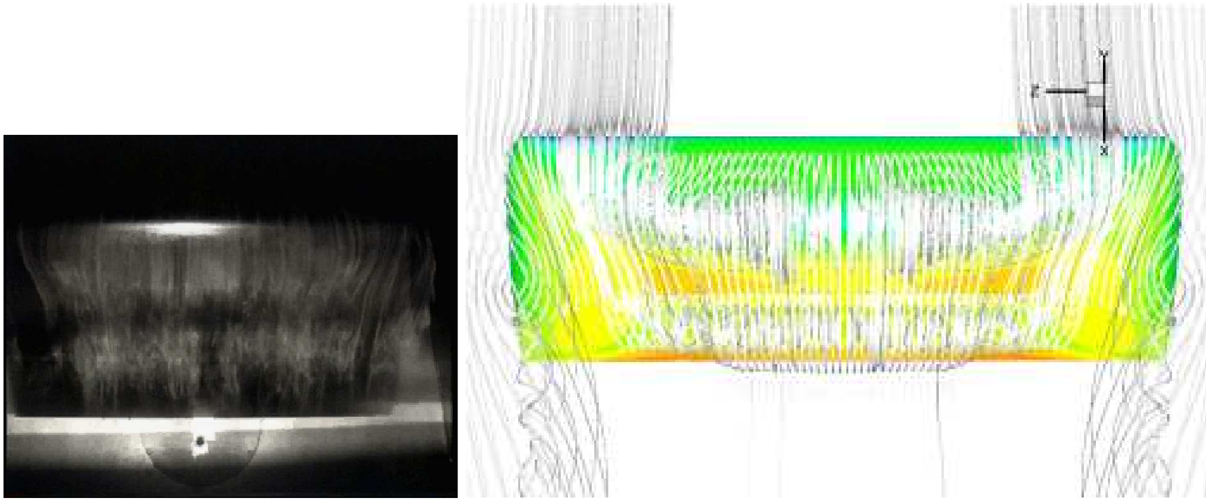

(a)

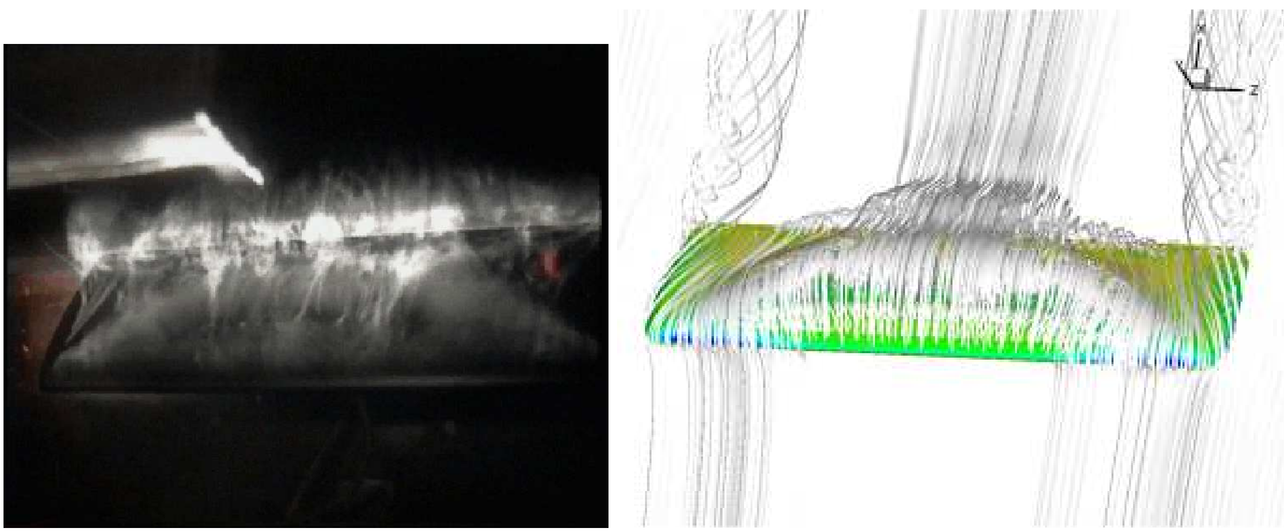

(b)

Figure 2: Smoke visualisation by Moir and Coton [11] (left) and CFD predictions (right) for the short aspect ratio wing of case 3 of Table 1. Ramping motion between 0^o and 40^o, Re=13,000, M=0.1, α^+=0.16. (a) Plan view and (b) side view of the DS and the trailing edge vortices at an incidence angle of 30^o.

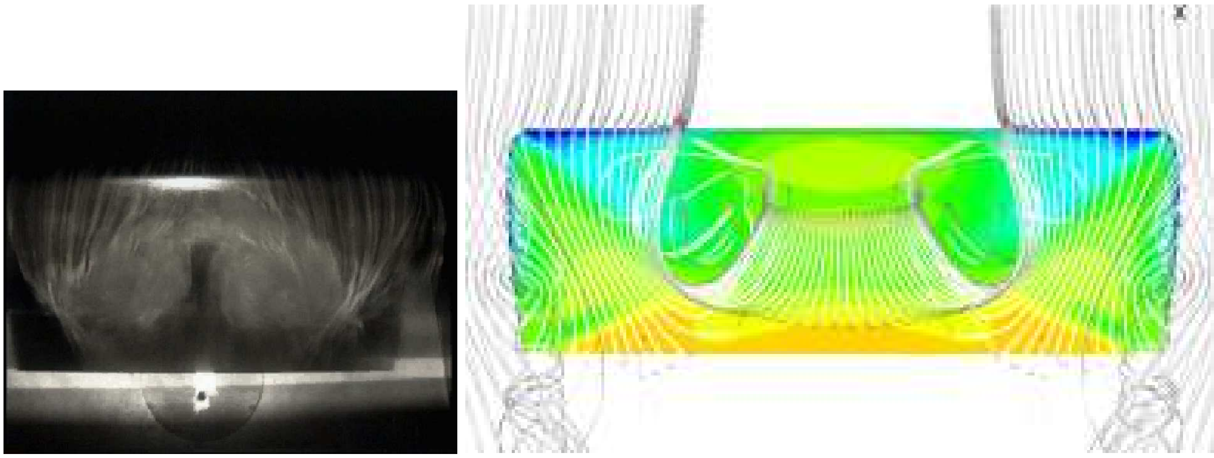

(a)

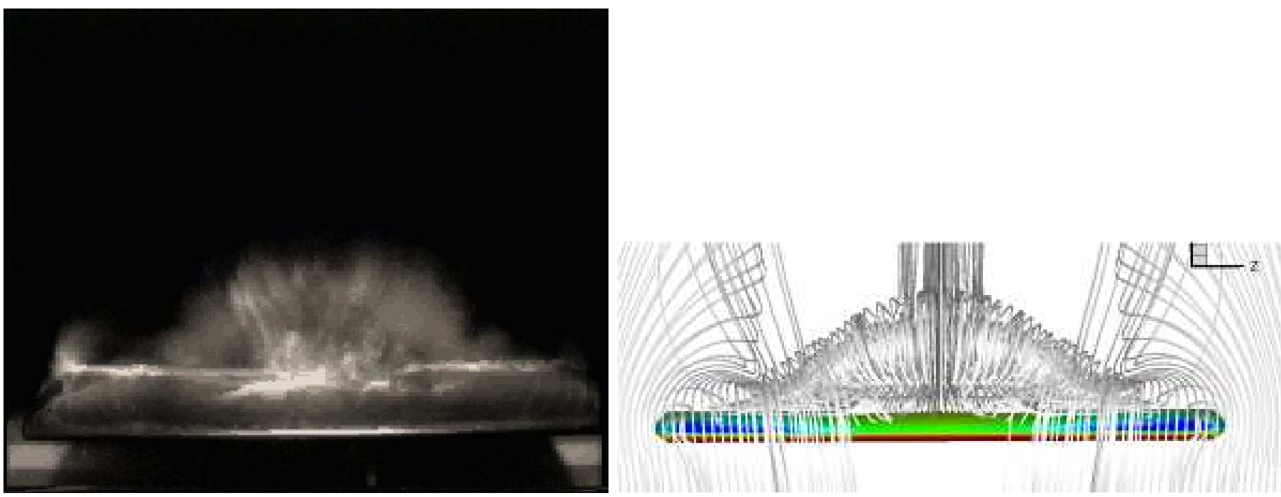

(b)

Figure 3: Smoke visualisation by Moir and Coton [11] (left) and CFD predictions (right) for the short aspect ratio wing of case 3 of Table 1. Ramping motion between 0^o and 40^o, Re=13,000, M=0.1, α^+=0.16. (a) Plan view and (b) view from the leading of the DS vortex at an incidence angle of 40^o.

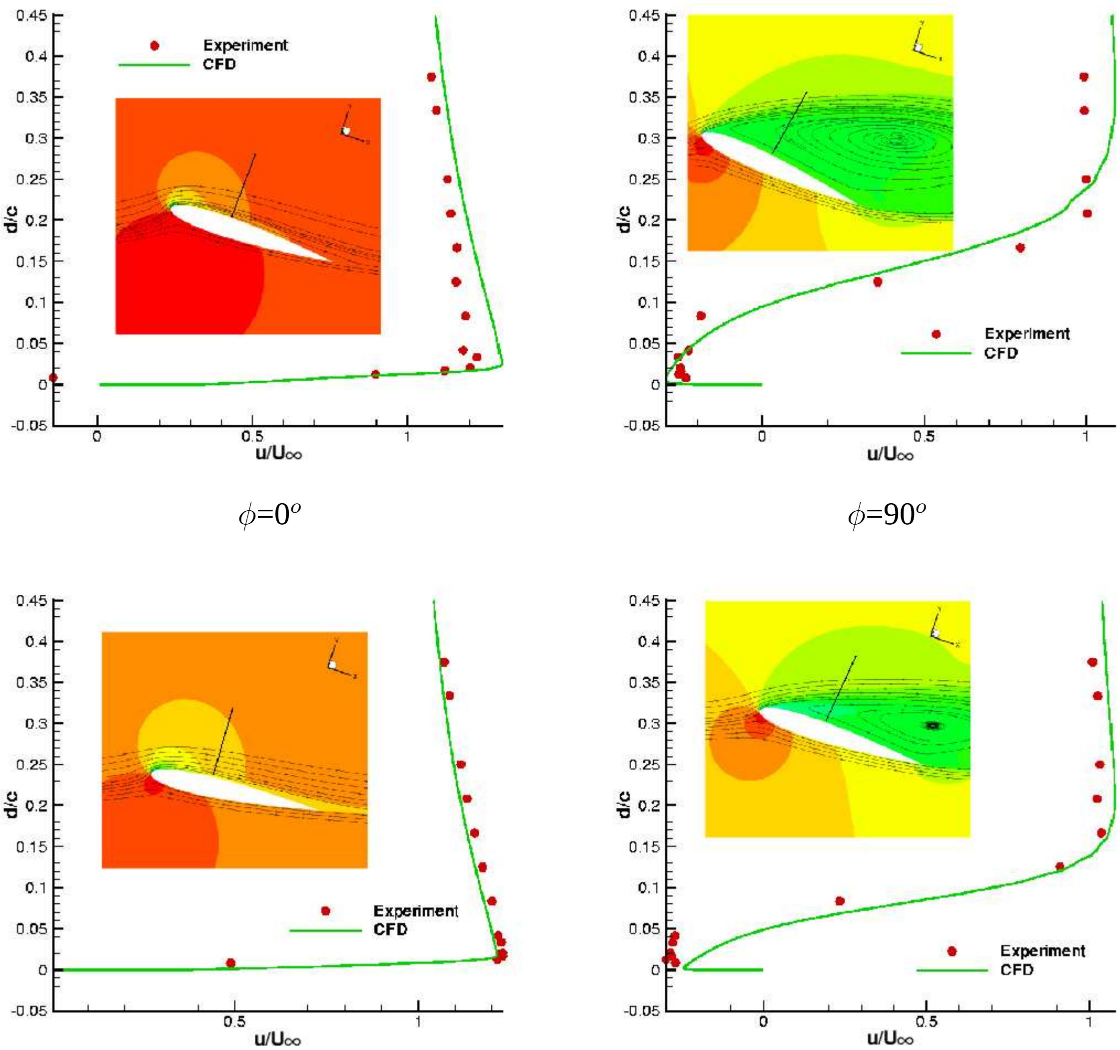

ϕ=0^o ϕ=90^o

ϕ=270^o ϕ=180^o

Figure 4: Comparison between CFD and ELDV measurements by Berton *et al.* [12] for the u-velocity profiles during DS. Oscillatory motion of a tapered wing, $\alpha(t) = 12^o + 6^o sin(kt)$, $k = 0.048$, $Re = 10^6$, $M = 0.2$. The line on the inserted plot corresponds to the direction of the ELDV probing, superimposed on pressure contours. The profiles were extracted at a spanwise sation of $z/c = 0.5$ and chordwise station of $x/c = 0.4$ (see Figure 1b).

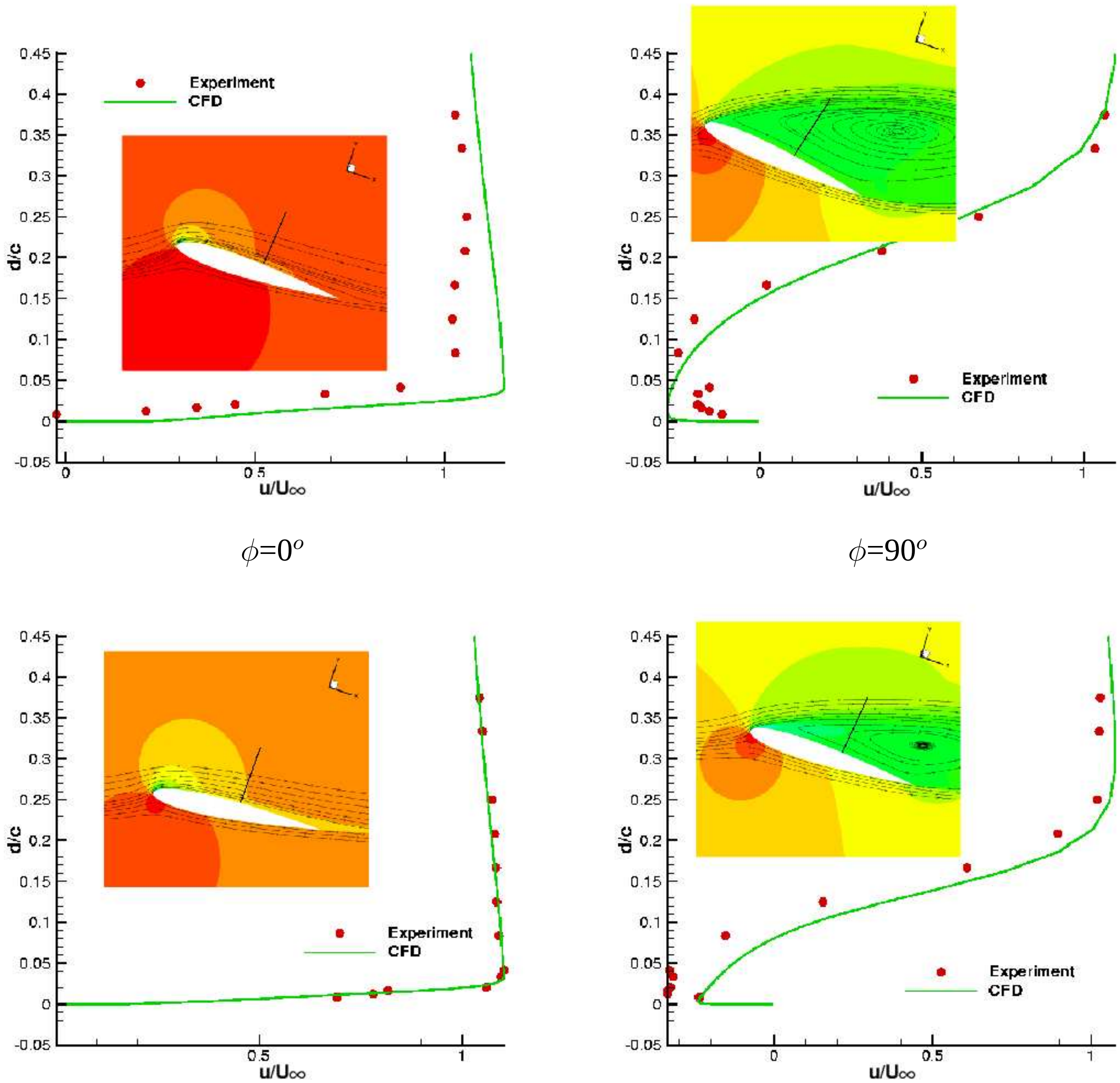

ϕ=0^o ϕ=90^o

ϕ=270^o ϕ=180^o

Figure 5: Comparison between CFD and ELDV measurements by Berton *et al.* [12] for the u-velocity profiles during DS. Oscillatory motion of a tapered wing, $\alpha(t) = 12^o + 6^o sin(kt)$, $k = 0.048$, $Re = 10^6$, $M = 0.2$. The line on the inserted plot corresponds to the direction of the ELDV probing, superimposed on pressure contours. The profiles were extracted at a spanwise sation of $z/c = 0.5$ and chordwise station of $x/c = 0.6$ (see Figure 1b).

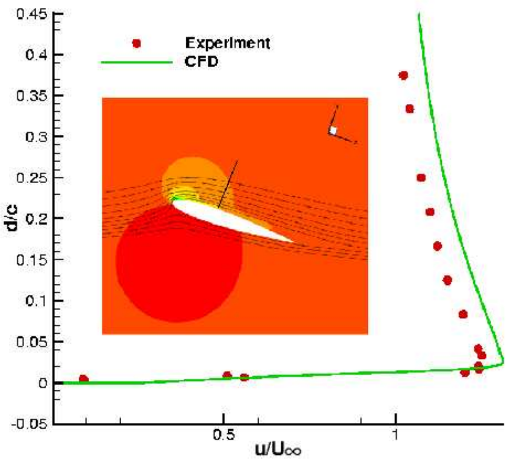

ϕ=0^o

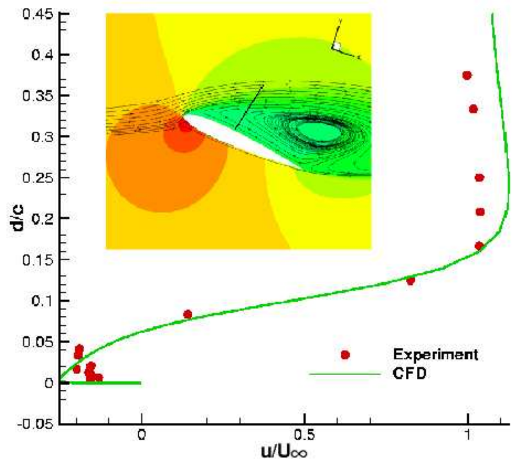

ϕ=90^o

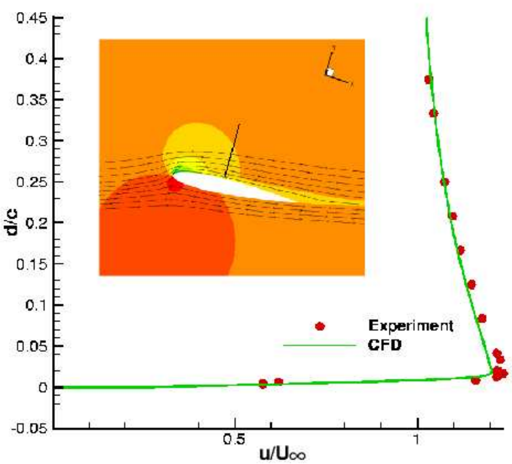

ϕ=270^o

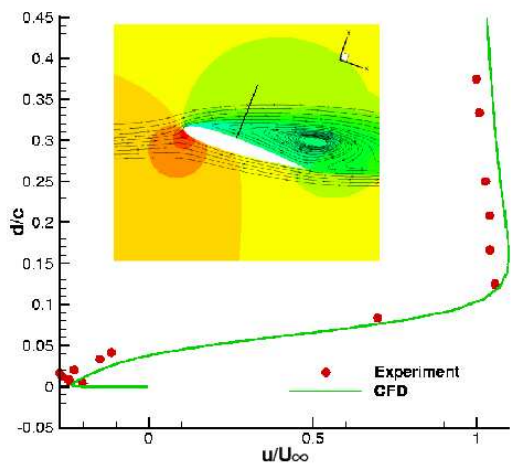

ϕ=180^o

Figure 6: Comparison between CFD and ELDV measurements by Berton *et al.* [12] for the u-velocity profiles during DS. Oscillatory motion of a tapered wing, $\alpha(t) = 12^o + 6^o sin(kt)$, $k = 0.048$, $Re = 10^6$, $M = 0.2$. The line on the inserted plot corresponds to the direction of the ELDV probing, superimposed on pressure contours. The profiles were extracted at a spanwise sation of $z/c = 0.7$ and chordwise station of $x/c = 0.4$ (see Figure 1b).

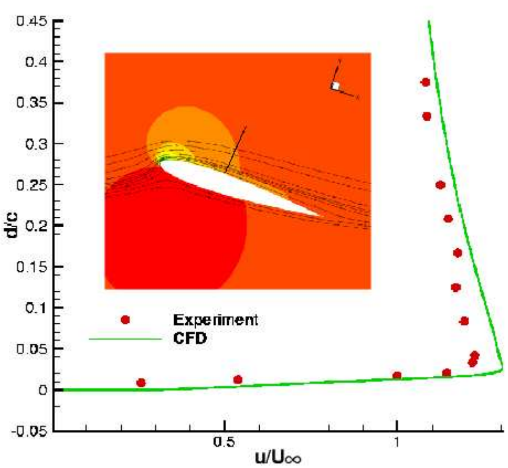

ϕ=0^o

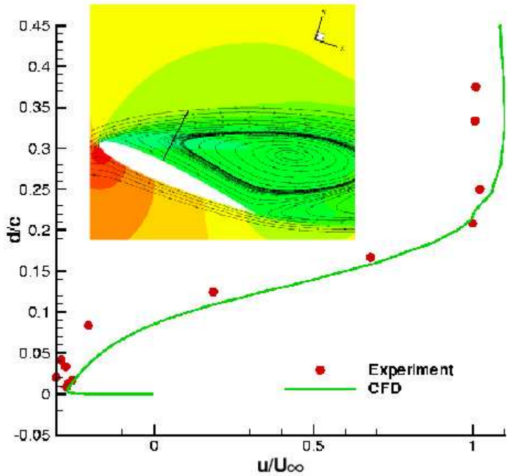

ϕ=90^o

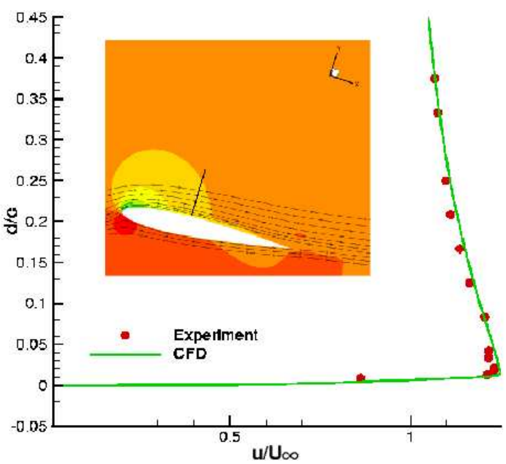

ϕ=270^o

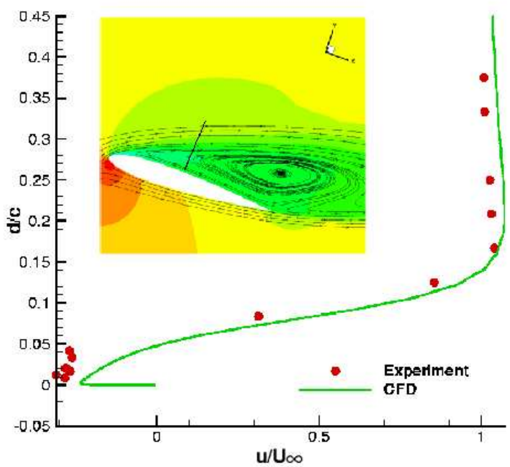

ϕ=180^o

Figure 7: Comparison between CFD and ELDV measurements by Berton *et al.* [12] for the u-velocity profiles during DS. Oscillatory motion of a tapered wing, $\alpha(t) = 12^o + 6^o sin(kt)$, $k = 0.06$, $Re = 10^6$, $M = 0.2$. The line on the inserted plot corresponds to the direction of the ELDV probing, superimposed on pressure contours. The profiles were extracted at a spanwise sation of $z/c = 0.5$ and chordwise station of $x/c = 0.4$ (see Figure 1b).

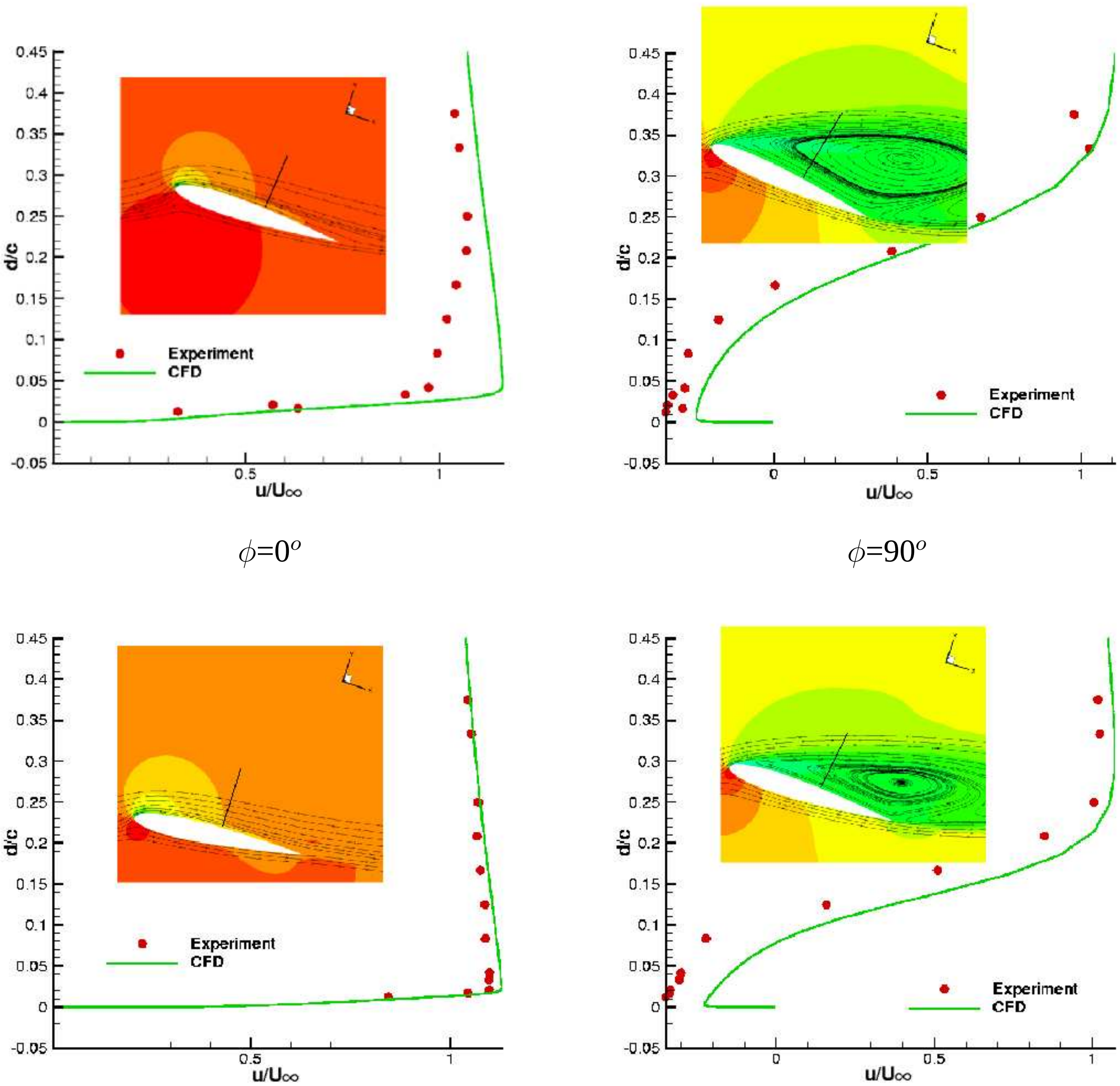

ϕ=0^o ϕ=90^o

ϕ=270^o ϕ=180^o

Figure 8: Comparison between CFD and ELDV measurements by Berton *et al.* [12] for the u-velocity profiles during DS. Oscillatory motion of a tapered wing, $\alpha(t) = 12^o + 6^o sin(kt)$, $k = 0.06$, $Re = 10^6$, $M = 0.2$. The line on the inserted plot corresponds to the direction of the ELDV probing, superimposed on pressure contours. The profiles were extracted at a spanwise sation of $z/c = 0.5$ and chordwise station of $x/c = 0.6$ (see Figure 1b).

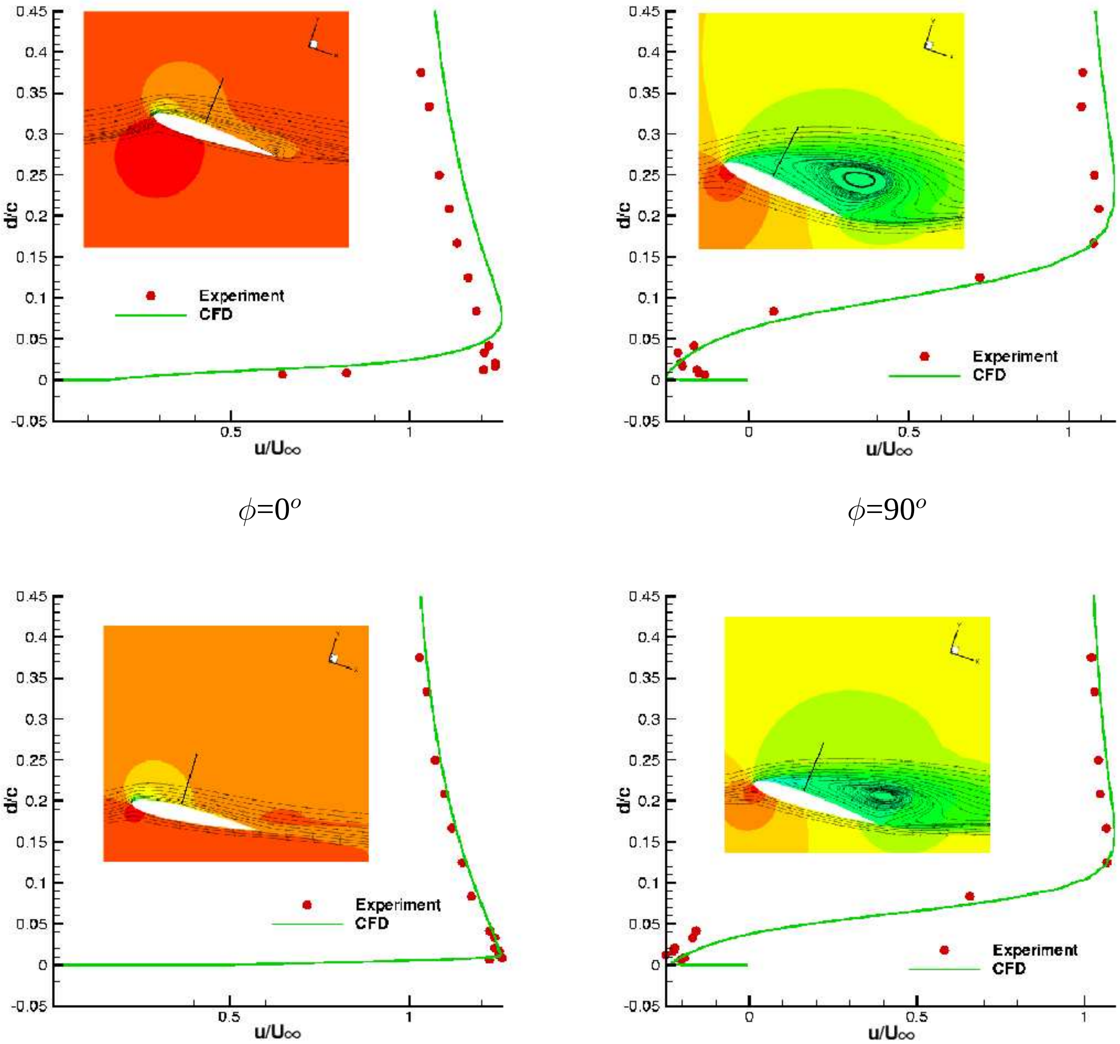

ϕ=0^o ϕ=90^o

ϕ=270^o ϕ=180^o

Figure 9: Comparison between CFD and ELDV measurements by Berton *et al.* [12] for the u-velocity profiles during DS. Oscillatory motion of a tapered wing, $\alpha(t) = 12^o + 6^o sin(kt)$, $k = 0.06$, $Re = 10^6$, $M = 0.2$. The line on the inserted plot corresponds to the direction of the ELDV probing, superimposed on pressure contours. The profiles were extracted at a spanwise sation of $z/c = 0.7$ and chordwise station of $x/c = 0.4$ (see Figure 1b).

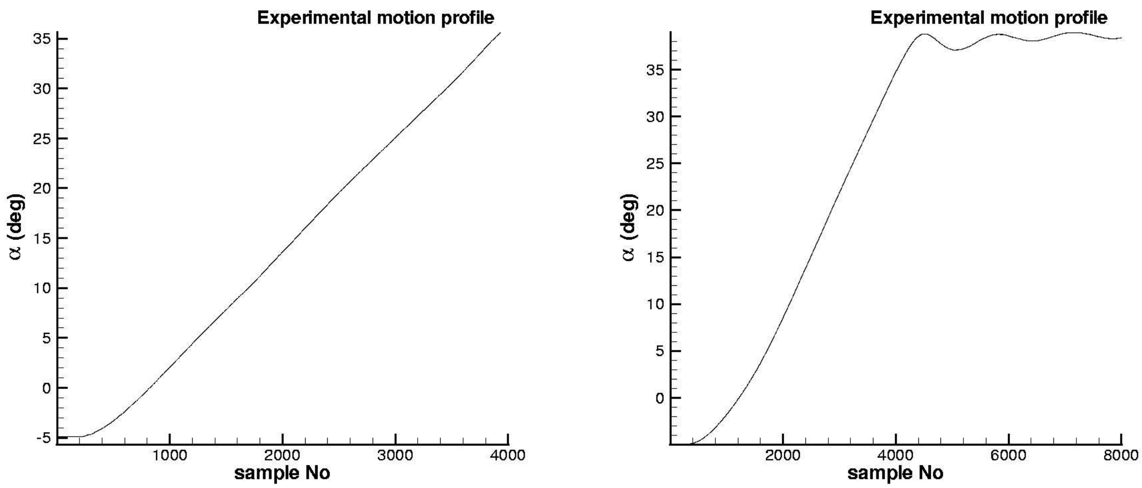

$\alpha^+ = 0.011$ (a) $\alpha^+ = 0.022$

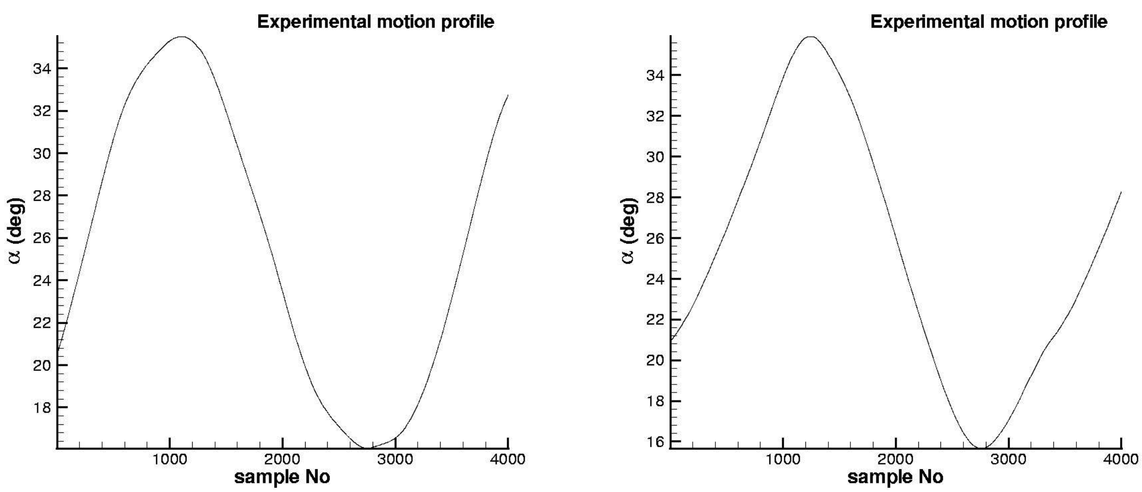

$k = 0.092$ (b) $k = 0.17$

Figure 10: Geometric angle vs sample number of the wing motion for the case by Coton and Galbraith [14]. (a) Ramping cases at $\alpha^+ = 0.011$ (left) and $\alpha^+ = 0.022$ (right). (b) Oscillatory cases at $k = 0.092$ (left) and $k = 0.17$ (right).

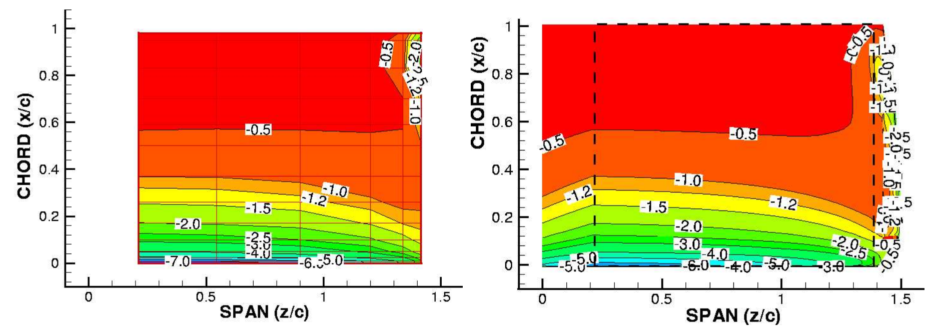

(a)

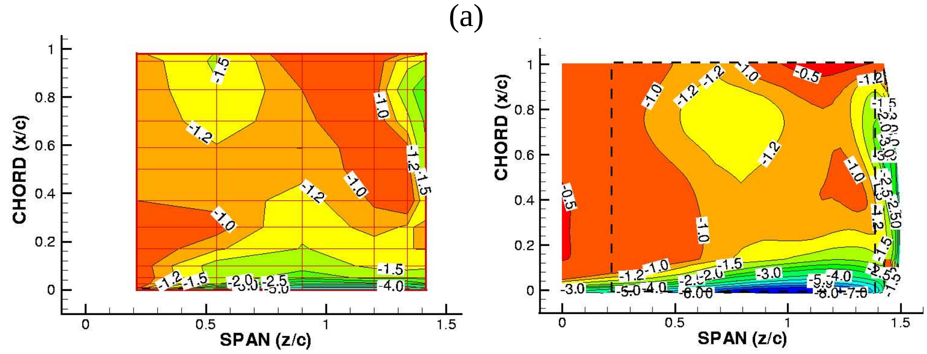

(b)

Figure 11: Comparison between experimental (left) and CFD (right) surface pressure distributions for the case 4 of Table 1 [14]. Ramping wing motion between -5^o and 39^o, $\alpha^+ = 0.011$, $Re = 1.5 \times 10^6$, $M = 0.16$. (a) $\alpha = 20^o$ and (b) $\alpha = 37^o$ (CFD), $\alpha = 32^o$ (Experiment).

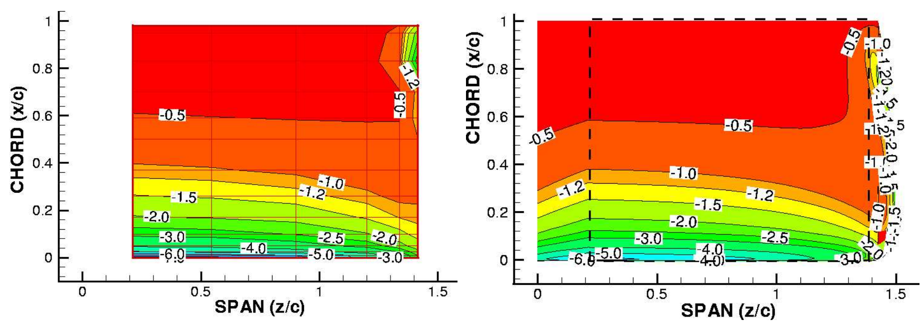

(a)

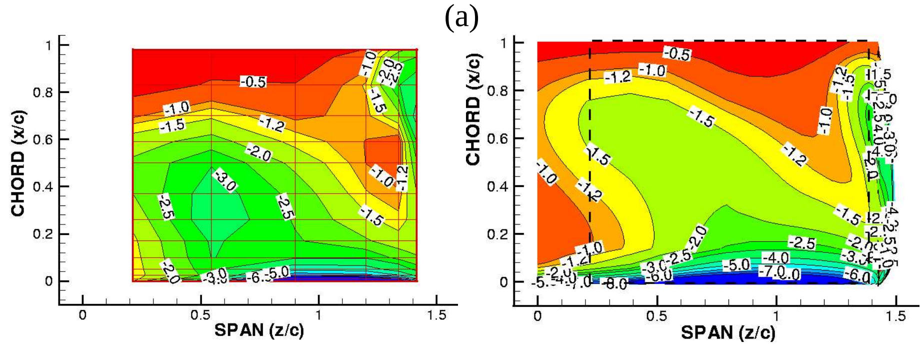

(b)

Figure 12: Comparison between experimental (left) and CFD (right) surface pressure distributions for the case 4 of Table 1 [14]. Ramping wing motion between -5^o and 39^o, $\alpha^+ = 0.022$, $Re = 1.5 \times 10^6$, $M = 0.16$. (a) $\alpha = 20^o$ and (b) $\alpha = 37^o$ (CFD), $\alpha = 33^o$ (Experiment).

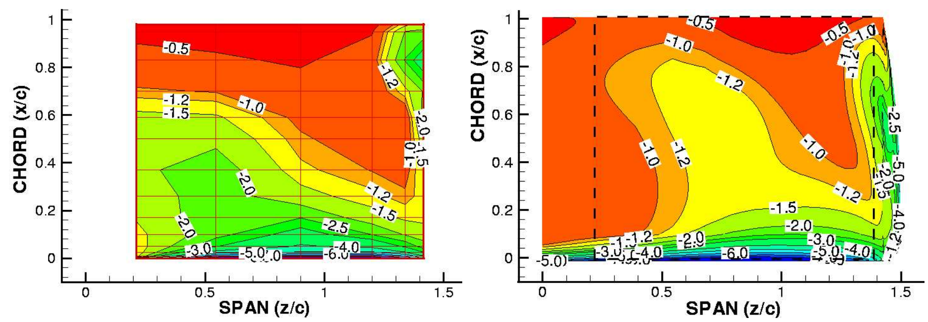

(a)

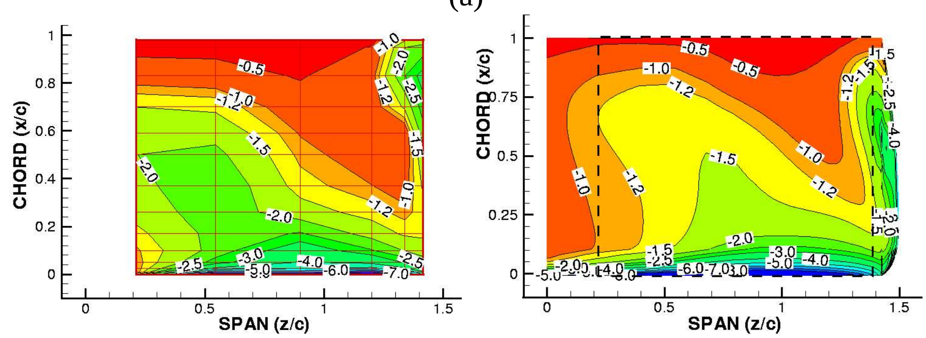

(b)

Figure 13: Comparison between experimental (left) and CFD (right) surface pressure distributions for the case 4 of Table 1 [14]. Oscillating wing motion between 15^o and 35^o, $Re = 1.5 \times 10^6$, $M = 0.16$. (a) $k = 0.092$, $\alpha = 34^o$ (CFD), $\alpha = 30^o$ (Experiment) and (b) $k = 0.17$, $\alpha = 35^o$ (CFD), $\alpha = 31^o$ (Experiment).

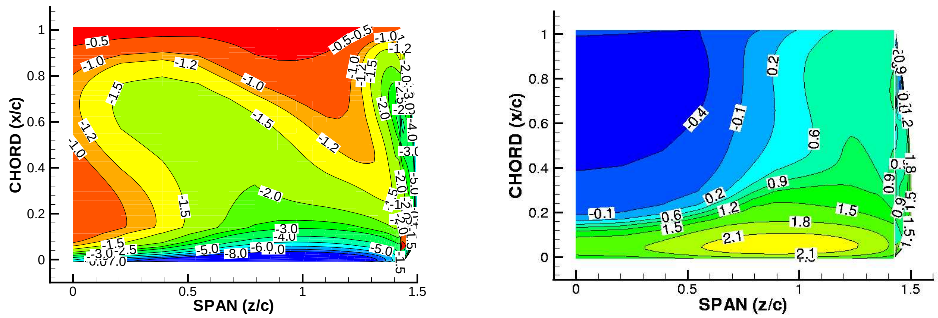

(a)

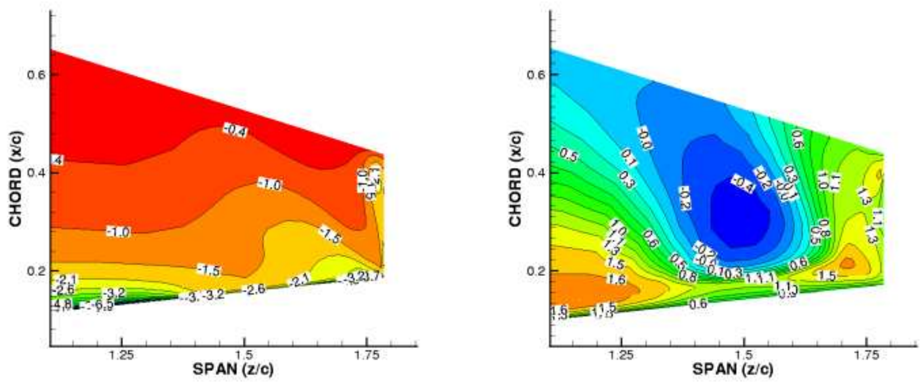

(b)

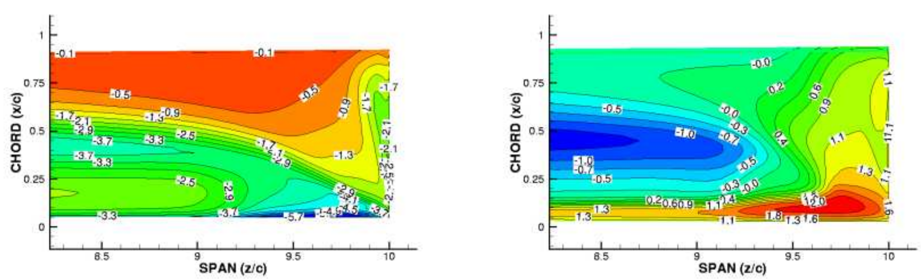

(c)

Figure 14: Cp (left) and u-velocity (right) contour plots near the stall angle. (a) Low aspect ratio wing with rounded tips [14], ramping motion between $\alpha = -5^o$ and $\alpha = 39^o$, $\alpha^+ = 0.022$, $Re = 1.5 \times 10^6$, $M = 0.16$, (b) tapered wing with flat tip [12], oscillatory motion, $k = 0.17$, $Re = 1.5 \times 10^6$, $M = 0.16$, (c) large aspect ratio wing with 10^o negative twist and flat tip, ramping motion between $\alpha = 0^o$ and $\alpha = 40^o$, $Re = 13,000$, $M = 0.16$, $\alpha^+ = 0.1$.

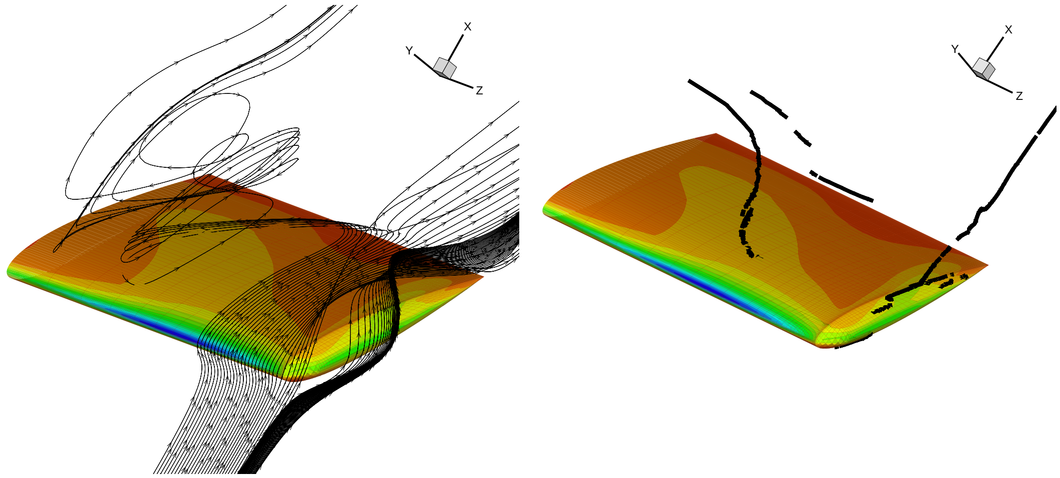

(a)

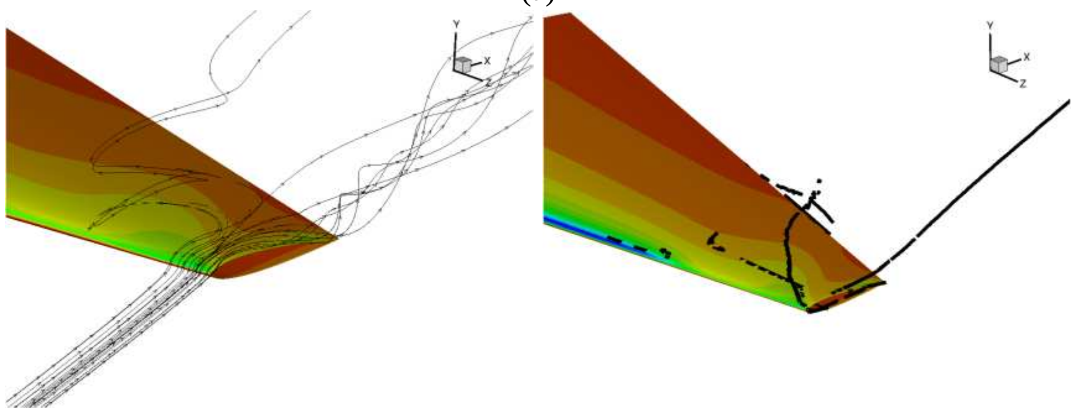

(b)

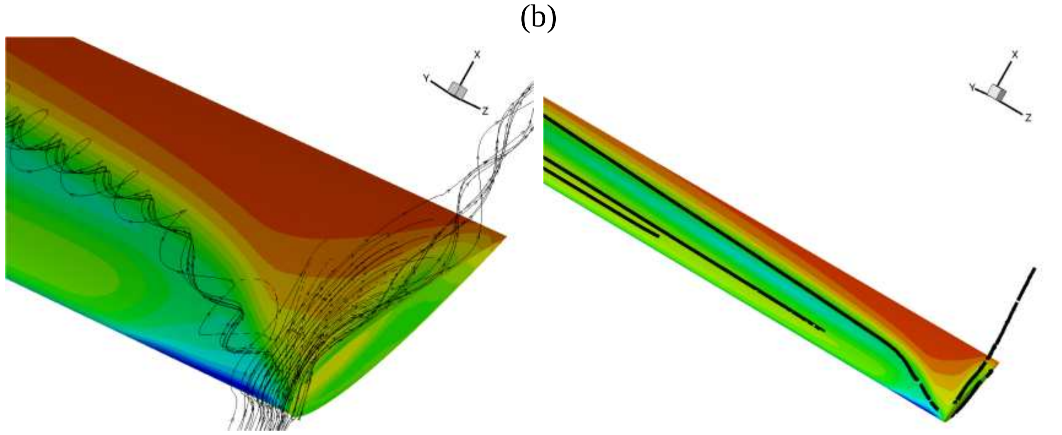

(c)

Figure 15: Streamlines (left) and vortex cores (right) near the stall angle. (a) Low aspect ratio wing with rounded tips [14], ramping motion between $\alpha = -5^o$ and $\alpha = 39^o$, $\alpha^+ = 0.022$, $Re = 1.5 \times 10^6$, $M = 0.16$, (b) tapered wing with flat tip [12], oscillatory motion, $k = 0.17$, $Re = 1.5 \times 10^6$, $M = 0.16$, (c) large aspect ratio wing with 10^o negative twist and flat tip, ramping motion between $\alpha = 0^o$ and $\alpha = 40^o$, $Re = 13,000$, $M = 0.16$, $\alpha^+ = 0.1$.